Molecular Imaging in the Framework of Personalized Cancer Medicine

Dževad Belkić PhD[1] and Karen Belkić MD PhD[1,2,3]

[1]Department of Oncology/Pathology, Karolinska Institute, Stockholm, Sweden
[2]Claremont Graduate University, School of Community and Global Health, and [3]Institute for Prevention Research, University of Southern California School of Medicine, Los Angeles, CA, USA

ABSTRACT: With our increased understanding of cancer cell biology, molecular imaging offers a strategic bridge to oncology. This complements anatomic imaging, particularly magnetic resonance (MR) imaging, which is sensitive but not specific. Among the potential harms of false positive findings is lowered adherence to recommended surveillance post-therapy and by persons at increased cancer risk. Positron emission tomography (PET) plus computerized tomography (CT) is the molecular imaging modality most widely used in oncology. In up to 40% of cases, PET-CT leads to changes in therapeutic management. Newer PET tracers can detect tumor hypoxia, bone metastases in androgen-sensitive prostate cancer, and human epidermal growth factor receptor type 2 (HER2)-expressive tumors. Magnetic resonance spectroscopy provides insight into several metabolites at the same time. Combined with MRI, this yields magnetic resonance spectroscopic imaging (MRSI), which does not entail ionizing radiation and is thus suitable for repeated monitoring. Using advanced signal processing, quantitative information can be gleaned about molecular markers of brain, breast, prostate and other cancers. Radiation oncology has benefited from molecular imaging via PET-CT and MRSI. Advanced mathematical approaches can improve dose planning in stereotactic radiosurgery, stereotactic body radiotherapy and high dose-rate brachytherapy. Molecular imaging will likely impact profoundly on clinical decision making in oncology. Molecular imaging via MR could facilitate early detection, especially in persons at high risk for specific cancers.

IMAJ 2013; 15: 665–672

KEY WORDS: molecular imaging, positron emission tomography (PET), magnetic resonance spectroscopic imaging (MRSI), radiation oncology, high cancer risk surveillance

Molecular imaging is an emerging medical discipline that integrates cellular and molecular biology with diagnostic imaging. It encompasses several imaging modalities that provide critical information for early detection and progression of disease, for predicting response to therapy and for evaluating treatment efficacy through its cellular and molecular pathways. Given the rapidly growing sophistication in our understanding of the cell biology of cancer, molecular imaging offers a strategic bridge to clinical oncology. It is of critical importance to non-invasively assess the behavior of tumors, for which in vivo molecular imaging is a key methodology. Molecular imaging detects not only the presence of the disease process, but can potentially also quantify its extent and severity, as well as follow the course of disease over time. Besides its diagnostic possibilities, molecular imaging is vital for target definition within dose-planning systems for radiotherapy. Molecular imaging is also an invaluable tool during and after therapy for assessing dose delivery and the overall success of treatment, as well as for deciding post-radiotherapy whether the patient needs further treatment and, if so, with which modalities. Recently, molecular imaging has proven to be pivotal, as well, for image-guided biopsy and surgery. This is particularly crucial since there may be multiple sites of cancer and image guiding can help detect them. Imaging is likely to become an important tool for cancer staging. Molecular targeting can be especially helpful in visualizing the extent of certain malignancies such as androgen-sensitive prostate cancers, neuroendocrine tumors, among others.

The strategic importance of molecular imaging in providing the best possible care for patients with or at risk for cancer has been emphasized [1-3]. As recently stated: "Molecular imaging is rapidly gaining recognition as a tool that has the capacity to improve every facet of cancer care. The growing demands among physicians, patients and society for personalized care are increasing the importance of molecular imaging and shaping the development of biomedical imaging as a whole." [3] (p. 182)

LIMITATIONS OF PURELY ANATOMIC IMAGING

Anatomic imaging is vital for cancer detection, as well as for staging and evaluation of response to therapy. Magnetic resonance imaging, ultrasound and computerized tomography are anatomic imaging modalities used routinely in clinical

practice in oncology. These modalities, particularly MRI, are generally quite sensitive, such that cancerous lesions are often identified. The most critical limitation of purely anatomic imaging is poor specificity, i.e., many non-malignant lesions will be detected, necessitating further investigation to distinguish them from cancers.

Among the potential deleterious consequences of false positive findings are unnecessary workup and procedures, adverse psychological effects, and expense. Psychological distress can lead to lower adherence to medical recommendations among patients who are monitored after treatment and among persons at high risk for certain cancers. A salient example is breast cancer screening, where false positive mammographic findings were found to be associated with decreased likelihood of attending subsequent screening [4,5]. Notwithstanding its superior sensitivity, the large number of false positive findings generated by MRI can have a negative impact. Indeed, in a study of women with elevated breast cancer risk and eligible to undergo breast MRI, only about 58% agreed to do so. Fear and concern about additional biopsies or testing were major reasons cited for refusal [6]. These issues are particularly relevant for programs monitoring women at high risk, for whom surveillance starts considerably earlier than for the general population [7].

PET COMBINED WITH CT

Positron emission tomography is the molecular imaging modality most widely used in current clinical practice in oncology. In combination with CT, anatomic and molecular imaging is achieved with PET-CT, which has had a major impact on the care of patients with cancer. A number of radiopharmaceuticals have been applied, with ^{18}F-fluoro-2-deoxy-D-glucose, a glucose analog, being the key biomarker. This is based on the fact that anaerobic glycolysis (the Warburg effect) is enhanced in cancer cells, as an early event. Thus, FDG is preferentially taken up by cancer cells as compared to normal cells and is used as a marker for malignancy.

Molecular imaging with PET-CT and MR-spectroscopic imaging offers more than anatomic imaging alone, particularly improved specificity for identifying cancers

It has been shown that whole-body PET-CT provides improved staging of cancer compared to anatomic imaging alone. In up to 40% of cases, application of PET-CT has led to changes in the treatment of patients with cancer [3,8,9]. PET-CT has also been useful in identifying the primary cancer site when the primary malignant lesion is unknown [3].

Within the framework of radiation treatment guidance, PET-CT has also been of vital importance. In-beam PET-CT cameras can monitor in situ dose depositions in the tumor. With this modality it would be possible to promptly introduce necessary corrections in the dose-planning system to amend the fractionation therapy in the subsequent dose delivery. To accomplish this goal, however, the following issue needs to be addressed; namely, how to achieve a proper connection between the activity curves and the dose distributions. This is a mathematically difficult ill-conditioned problem within the realm of reconstructions, for which the correct solution has not yet been found. The PET-CT camera is used today in light ion radiotherapy with the primary particle beam which can generate secondary nuclei that emit positrons (e.g., ^{12}C is transmuted to the β^+ emitters ^{11}B and ^{10}B). This type of in situ monitoring of dose distributions could provide invaluable information about the patient's response to irradiation. The response should be used interactively to appropriately modify the simulation codes and thus optimize dose delivery. FDG-PET has also been used to identify areas of hyper-metabolism for which a boost dose of radiation may be indicated [3,10,11].

Besides FDG-PET, other tracers such as ^{18}F-3'deoxy-3'-fluorothymidine and ^{18}F-fluoro-miso-nidazole have been used in certain indications. FLT-PET appears to be advantageous in brain tumor diagnostics since it has less physiological uptake than FDG-PET [3]. For identifying tumor cell hypoxia, a recognized cause of treatment resistance, F-MISO-PET has been reported to help guide combined chemotherapy and radiation therapy in patients with head and neck tumors [12].

Notwithstanding these remarkable advances offered by molecular imaging with PET-CT, there are limitations, particularly the lack of specificity of the individual radiotracers. FDG is taken up by non-malignant cells, especially in the presence of inflammation. FLT is also taken up by benign reactive processes [13]. Newer molecular tracers that can further improve the diagnostic accuracy of PET are emerging. Among these are ^{68}Ga-DOTATOC for imaging neuroendocrine tumors and ^{18}F-fluoro-dihydrotestosterone, an anti-androgen receptor, which detects bone metastases in androgen-sensitive prostate cancer that remain unrecognized by FDG-PET or bone scans [3]. Progress is being made in finding the best tracer for PET imaging of human epidermal growth factor receptor type 2 (HER2)-expressive tumors [14]. The results of these studies hold promise for stratifying patients to appropriate therapy and for predicting prognosis. There have also been attempts to use multiple tracers to improve the diagnostic accuracy of PET-CT [3]. Further steps should be aimed at introducing the most promising of the new molecular PET tracers or their combinations into the clinical protocol, so that patients with cancer can maximally benefit from these advances. Ever closer linkage is needed between molecular imaging via PET-CT and the established and emerging "hallmarks of cancer" [15].

PET = positron emission tomography
FDG = ^{18}F-fluoro-2-deoxy-D-glucose
FLT = ^{18}F-3'deoxy-3'-fluorothymidine
F-MISO = ^{18}F-fluoro-miso-nidazole

MRI COMBINED WITH SPECTROSCOPY

Combined molecular and anatomic imaging can be achieved by a strategy different from that of PET-CT. Namely, magnetic resonance spectroscopy can be combined with MRI to yield MR spectroscopic imaging. Until recently, MRSI has mainly been performed on an individual organ or tissue, most notably in neuro-oncology, i.e., for detecting, characterizing and treating brain tumors [16,17]. MRS and MRSI have also been applied extensively in the initial detection of prostate cancer, distinguishing high from low risk lesions, as well as staging, treatment planning, and surveillance for residual cancer and local recurrence after therapy [16]. MRS and MRSI have also been used in the diagnosis and treatment of breast cancer, sarcomas, head and neck cancers and other malignancies [3,18,19].

A major advantage of MR-based modalities is the lack of exposure to ionizing radiation. This is a vital consideration, especially when repeated monitoring is needed. It is of critical importance for the pediatric population. Also, for persons at increased risk for cancer, MR-based surveillance at more frequent intervals starting at a younger age would thereby become safer and thus more feasible.

Molecular imaging can improve all aspects of clinical cancer care

Unlike most applications of PET, diagnostics by MRS and MRSI can provide insight into a number of metabolites at the same time. Among these, choline, with a resonant frequency at ~3.2 ppm (parts per million), has been especially informative as a reflection of phospholipid metabolism of cell membranes and as a marker for membrane damage, cellular proliferation and cell density, as typically seen in malignancy.

Figure 1 shows how MRS can improve the specificity of MRI. Figure 1A shows two hyperlucent, practically indistinguishable lesions on T_2-weighted MRI. The metabolic information provided by MRS (Figure 1B) suggests that the lesion with the arrow is malignant, as subsequently confirmed on histopathology as low grade astrocytoma. The two hyperlucent lesions on the MRI look very much alike anatomically, but not metabolically. Hence these chemical changes, which are not visible on MRI, can be detected and quantitatively evaluated by MRS and/or MRSI. In this way, MRSI complements MRI, yielding invaluable diagnostic information on metabolism of the tumorous tissue, often before changes can be identified with fidelity on conventional anatomic images. Detecting a small size tumor with confidence by MRSI is of utmost importance since it enables the selection of appropriate treatment at an early stage of disease.

A number of institutions have higher magnetic field scanners dedicated to clinical oncology. Thereby, MRS and MRSI, as well as functional techniques such as diffusion-weighted MRI, can be more widely incorporated into the diagnostic and therapeutic protocols for patients with various malignancies. At this higher magnetic field strength, the resolution and signal-to-noise ratio are substantially enhanced; these are two important considerations for the clinical application of MRS and MRSI. By the same token, however, deterioration in the resolution of heavily overlapping resonances with the accompanying so-called spectral crowding also occurs in MR spectra at higher field strengths relative to 1.5T.

Instead, we are pursuing a less traveled road by exploring the alternative of gaining resolution improvement in MRS with ordinary 1.5T scanners by means of better equipped mathematics, via the fast Padé transform for optimization of signal processing. Our results applying the FPT demonstrate that in vivo MRS data encoded on 1.5T scanners can yield quantitative information on at least 25 brain metabolites [20], many of which could be diagnostically important for neuro-oncology. Further studies using the FPT suggest that a comparable diagnostic yield may also be possible for breast, prostate and ovarian cancers [21]. In other words, until recently, in vivo MRS and MRSI made great strides in clinical oncology by relying on a mere handful of metabolites, or even a single metabolite, e.g., total choline for breast cancer. By expanding this severely restricted metabolite window, through translation of basic science knowledge to clinical MRS and MRSI, a more refined molecular imaging could allow a "personalized molecular fingerprint of individual tumors, as a basis for novel treatment algorithms" [3] (p.183).

Such an approach could be applied, for example, to detect the "glycerophosphocholine to phosphocholine switch," which according to human breast cell line research occurs with malignant transformation and is associated with over-expression of the enzyme choline kinase responsible for phosphocholine

FPT = fast Padé transform

MRSI = magnetic resonance spectroscopic imaging
MRS = magnetic resonance spectroscopy

Figure 1. [A] T_2-weighted MRI shows two similar-appearing hyperlucent lesions. **[B]** Spectrum obtained via MRS from the lesion marked with the arrow in [A]. The high ratio of choline (Cho) to creatine (Cr) and of choline to N-acetyl-aspartate (NAA) suggested malignancy. Histopathology confirmed this with the finding of a low grade astrocytoma. The abscissa in the right panel is a chemical shift as a dimensionless frequency in parts per million (ppm); the ordinate is intensity in arbitrary units (au)

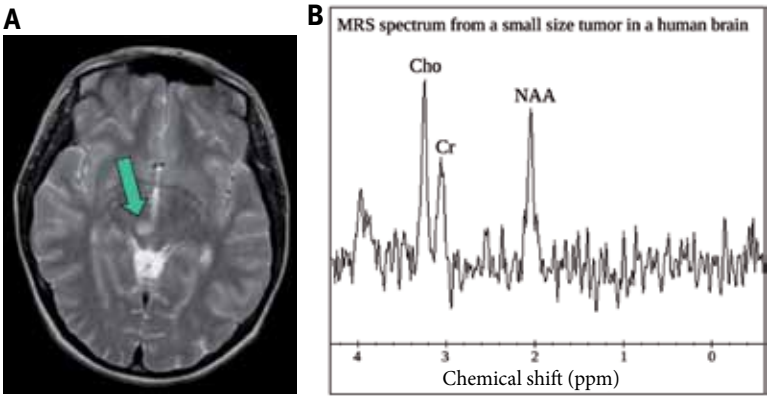

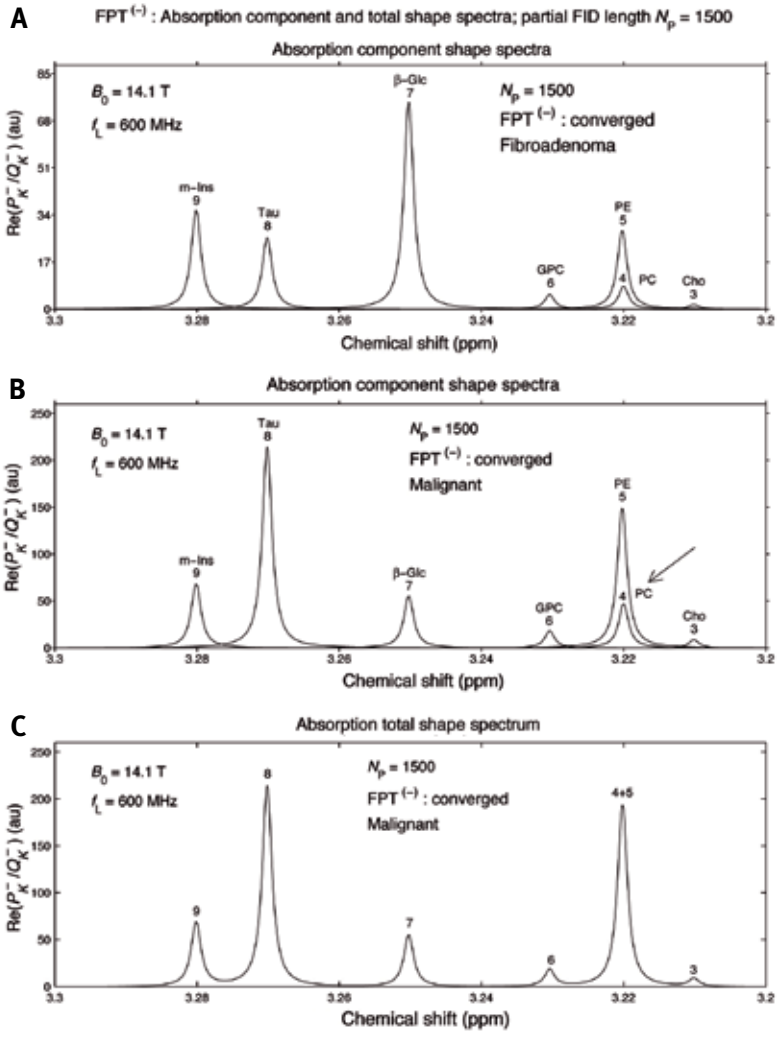

Figure 2. Absorption component shape spectra reconstructed by the fast Padé transform (FPT) [21] for fibroadenoma **[A]** and breast cancer **[B]** based on in vitro data from Ref. [39]. The arrow points to phosphocholine (PC), a marker of malignant transformation in the breast, which completely underlies phosphoethanolamine (PE). On the absorption total shape spectrum for breast cancer **[C]**, phosphocholine (peak #4) cannot be detected at all underneath PE (peak #5). Instead, a taller composite peak appears without any suggestion that this is actually the sum of peaks (##4+5). The components of total choline: glycerophosphocholine (GPC), choline (Cho) and phosphocholine, all lie closely within the interval of 3.21 ppm and 3.23 ppm. Other metabolites within the interval of 3.2 ppm and 3.3. ppm, as reconstructed by the FPT, include β-glucose (β-Glc), taurine (Tau) and myoinositol (m-Ins). The abscissa is in arbitrary units (au)

synthesis [22-24]. This reflects changes in membrane choline phospholipid metabolism. The main steps in choline metabolism occur via the cytosine diphosphate-choline pathway [22-24]. Within that pathway, choline (3.21 ppm), PC (3.22 ppm) and glycerophosphocholine (3.23 ppm) can be detected in the proton magnetic resonance spectrum, insofar as more advanced signal processing methods such as the fast Padé transform are used, as illustrated in Figure 2. Thus, it is necessary to analyze the relationship of these closely overlapping resonances, including phosphoethanolamine, which completely overlies PC. When choline, PC and GPC are summed up as "total choline," as is conventionally done with in vivo MRS, relevant information for breast cancer diagnostics may be missed. Studies suggest that the problem of overlapping resonances could be resolved by the FPT applied to in vivo MRS time signals. This could help improve breast cancer diagnostics and care of patients with breast cancer [21,25].

A wider application of proton MRS and MRSI is entirely feasible since they can be performed with the same equipment (radiofrequency coils, amplifiers, etc.) that is used for standard MRI. The practical clinical aspect, including economics, should also be emphasized, namely that 1.5T scanners are abundant in hospitals worldwide due to their purchase price, which is considerably lower than higher field scanners. Moreover, better-equipped mathematics via the FPT provide not only exact quantification of MRS data but can also fundamentally change the way MRS time signals are encoded. Overall, the FPT has a significant advantage in signal-to-noise ratio compared to conventional fast Fourier transform. This is because the FPT needs only short time signals compared to conventional acquisitions using the fast Fourier transform [21]. For short time signals, the FFT gives uninterpretable spectra [21]. As such, the new encoding of short time signals will presuppose the use of the FPT. Thus, the FPT directly influences how MR time signals should be encoded to enhance the overall performance of MRS. Further investigations comparing the resolution provided by the FPT using MRS/MRSI data encoded at 1.5T with that of higher field MR scanners are therefore needed. This is a key step for widespread and cost-effective implementation of mathematically optimized MRS/MRSI for diagnostics and various aspects of patient care in oncology.

MRSI IN RADIATION ONCOLOGY

Magnetic resonance spectroscopic imaging has also been widely used in radiation neuro-oncology and for radiation therapy of prostate cancer: for target definition, for identifying high grade regions that may benefit from boost doses, and for post-therapy follow-up [3,26]. MRSI has been particularly helpful in distinguishing between recurrent brain tumors and radiation necrosis post-radiotherapy [27]. Assessment of the response to chemotherapy may also be facilitated by MRS and MRSI so that prompt adjustments can be made [28,29]. Early detection of post-therapy residual cancer via MRSI, hence early intervention, will improve patient outcome. Empiric evidence is strongest to date for primary brain tumors and prostate cancers [3]. As illustrated in Figure 3, with advances in signal processing

PC = phosphocholine

GPC = glycerophosphocholine
FFT = fast Fourier transform

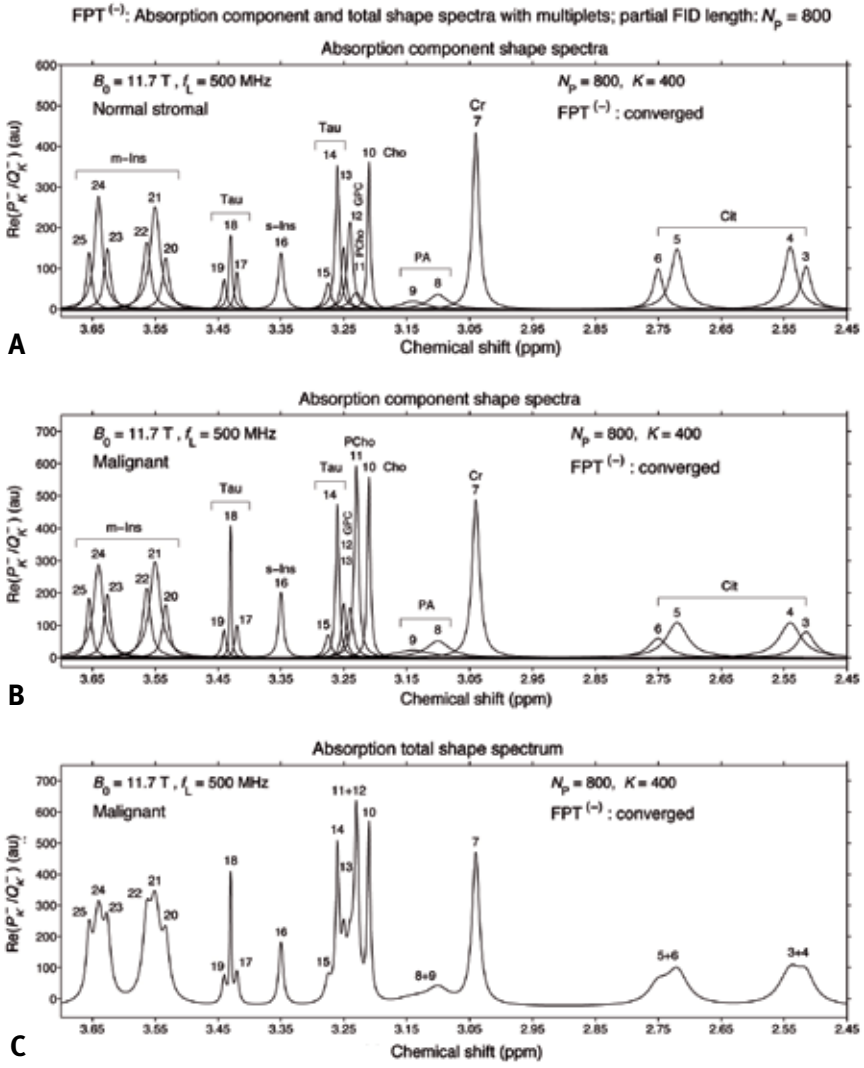

Figure 3. Absorption component spectra reconstructed by the fast Padé transform (FPT) [21] for normal stromal prostate **[A]** and malignant prostate **[B]** within the region 2.4–3.7 ppm based on in vitro data from Ref. [40]. Note the presence of several multiplet resonances whose component peaks are clearly delineated. The absorption total shape spectrum for malignant prostate is shown in **[C]**. There, by comparison, several of the multiplets, notably the doublets of citrate (peaks ##3+4, ##5+6) and of polyamines (##8+9) would be exceedingly difficult to identify and quantify. Moreover, phosphocholine and glycerophosphocholine (##11+12) can only be distinguished on the component shape spectrum. As discussed in the text, phosphocholine is a marker of malignant transformation (see also Figure 2). The abscissae are in dimensionless units of parts per million and the ordinates are in arbitrary units (au). Acronyms for metabolites: m-Ins = myoinositol, Tau = taurine, GPC = glycerophosphocholine, PC = phosphocholine, Cho = choline, PA = polyamines, Cr = creatine, Cit = citrate

through the FPT, a substantial number of informative peaks, including several multiplet resonances, can be delineated. These help distinguish prostate cancer from normal stromal prostate tissue, as seen in Figure 3A and B. This distinction is far more difficult, if not impossible, to make on the basis of the total shape spectrum, as illustrated in Figure 3C.

Evaluation of prognosis has also been greatly aided by MRS and MRSI, particularly for patients with primary brain tumors [30]. With the advances in signal processing, MRS and MRSI could also provide a quicker assessment of the success of radiotherapy and more expedient evaluation of any new lesions that arise post-radiotherapy [27]. Clearly, this information will translate into more timely and effective treatment steps.

Whole-body imaging through MRI and MRSI has been relatively limited until recently, due in part to their susceptibility to motion from respiration and peristalsis [3]. However, recent results indicate that whole-body MRI and MRSI may become feasible and could be applied to various aspects of cancer diagnostics and treatment [31].

Entailing no ionizing radiation exposure, molecular imaging with MR is suitable for surveillance of persons at increased cancer risk and post-therapy at frequent intervals, particularly children

ADVANCES IN MOLECULAR IMAGING FOR DOSE PLANNING IN RADIOTHERAPY

Combined modalities of PET and MRI may also be a promising avenue, particularly in light of the superior resolution, soft tissue contrast and multi-planar capabilities of MRI, together with its lack of ionizing radiation exposure, as mentioned. Such integrated PET-MR units are currently in development and initial

Figure 4. Cell survival as a function of dose *D* for Chinese hamster V79 cells irradiated by 250 kVp X-rays. **[A]** Cell-surviving fractions $S_F(D)$ versus *D* (Gy). Experiment (filled circles): Ref. [36]: Theories; full line: PLQ (Padé Linear Quadratic) model and dashed line: LQ (Linear Quadratic) model. **[B]** Full-effect (Fe) plot given by the product of the reciprocal dose $1/D$ and the negative natural logarithm of $S_F(D)$ as the ordinate $Fe(D)=-(1/D)\ln(S_F)$ versus *D* as the abscissa: Experiment (filled circles): Ref. [36]. Theories; full line: PLQ model and dashed line: LQ model (the straight line $\alpha+\beta D$)

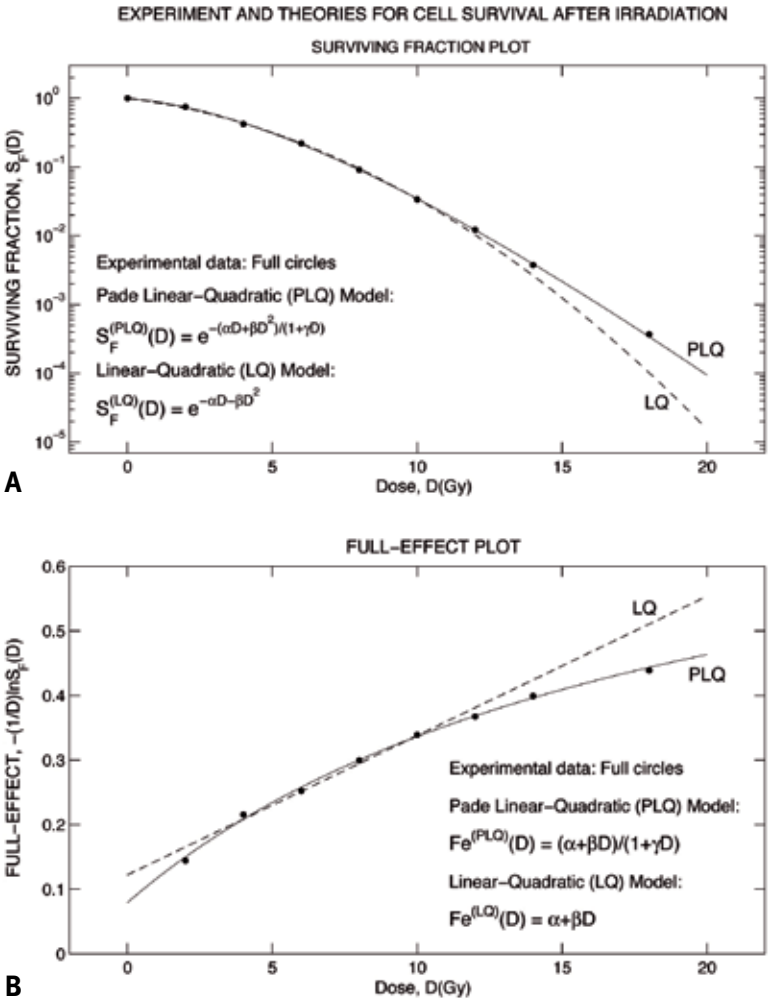

clinical applications have been reported [32]. An ongoing clinical trial is using ^{18}F-FMISO dynamic PET-CT and functional MRI for imaging tumor hypoxia in locally advanced unresectable non-small cell lung cancer. Inverse planning of radiation therapy is thereby carried out [33]. CT-MRI can verify whether irradiation to the clinical target volume in prostate cancer has been delivered as planned, with lowered chance of complication to the bladder and rectum which are the key organs at risk [34].

Further connections between MR diagnostics and dose-planning systems in radiotherapy are being developed within this framework. Cell survival fractions are being used to assess changes in MRS-quantified metabolite concentrations after radiotherapy [35]. This can help delineate the target volume for patients who require further radiation therapy after initial treatment. Experimental data exist on integral intensities of spectral line shapes with the underlying concentrations of a number of diagnostically relevant metabolites such as choline, N-acetyl aspartate, creatine, etc., as a function of the absorbed dose. To apply this information, an appropriate radiobiological model is needed for quantification of dose-effect relationships for doses ranging from low through intermediate to high. However, current dose-planning systems have been based on the Linear Quadratic model, which is limited to low doses and systematically underestimates the experimentally observed terminal exponential tail of the cell-surviving curves at high doses. This difficulty is especially relevant to hypofractionation (e.g., stereotactic radiosurgery) where high doses per fraction are usually delivered. It has been widely recognized that the success of radiotherapy ultimately depends on the proper assessment of cell repair. A new radiobiological formalism called the Padé Linear Quadratic model for cell survival using the Michaelis-Menten enzyme catalysis mechanism for cell repair was recently introduced. The PLQ model circumvents this difficulty and can be successfully applied to the entire dose range of interest [35], as illustrated in Figure 4. This advanced model enables more accurate dose planning for stereotactic radiosurgery, stereotactic body radiotherapy and high dose-rate brachytherapy. Figure 4 tests the PLQ by comparing its predictions with the experimental data for Chinese hamster cell lines irradiated by 250 kVp X-rays [36]. For our earlier applications of the PLQ model to different cell lines, see Ref. [35,37,38]. Both cell-surviving fractions $S_F(D)$, as dose-effect curves in Figure 4A, and the corresponding relative radiosensitivities of the cell, as the Fe-plots (full effect) in Figure 4B, are used in these comparisons between the measured and predicted quantities. The results are shown using the linear axis for dose *D* on the abscissa, whereas the ordinates are either logarithmic or linear for the $S_F(D)$ curve or the Fe plot, respectively. It can be seen from these two panels that throughout the entire dose range (0–18 Gy) the cell-surviving fractions and the Fe-plot in the PLQ model are in excellent agreement with the corresponding experimental data [38].

By contrast, as evidenced in Figure 4A, the LQ model for the S_F curve is valid only at low-to-intermediate doses (below 10 Gy). However, at higher doses shown in Figure 4A, the leading Gaussian shape of the dose-effect curve in the LQ model severely underestimates experimental data which exhibit a purely exponential behavior.

This breakdown of the LQ model is most prominently evidenced in the Fe-plot depicted in Figure 4B. Here, the LQ model

PLQ = Padé Linear Quadratic
LQ = Linear Quadratic

predicts a straight line $\alpha + \beta D$. Geometrically interpreted, the parameter α is the intercept of the straight line $Fe = \alpha + \beta D$ with the ordinate, whereas β is the slope of this line. This straight line behavior indicates that the full effect will continuously increase without limit by augmentation of dose D. Any departure of experimental data from this pattern would imply inadequacy of the LQ model. This is precisely what is observed in Figure 4B, where the measured findings for the Fe-plot strongly deviate from the LQ-based straight line both at lower and higher doses. Simultaneously, it is clear from Figure 4B that the pertinent prediction of the PLQ model for the Fe-plot is in excellent accord with the associated experimental data at all doses.

In contrast to the straight line $Fe = \alpha + \beta D$ in the LQ model, the Fe-plot in the PLQ model is given by the rectangular hyperbola $Fe = (\alpha + \beta D)/(1 + \gamma D)$, which fully describes the experimental data in Figure 4B. While the LQ-based Fe-plot for the relative radiosensitivity is an ever-increasing function with augmented dose according to $Fe = \alpha + \beta D$, the PLQ-designed counterpart via $Fe = (\alpha + \beta D)/(1 + \gamma D)$ is seen to saturate at asymptotically large D by attaining a constant value β/γ, which can be identified with the reciprocal of the mean lethal dose D_0.

The current practice in a dose-planning system is to use the LQ model in evaluating the biologically effective dose, $BED_{LQ} = 1 + (\beta/\alpha)\, D$. The BED is most useful in fractionation radiotherapy. In particular, the concept of the BED is considered of critical importance for determining the dose per fraction for non-conventional fractionations (larger doses per fraction in stereotactic radiosurgery, for example) by extrapolating the abundant experience from conventional fractionation (smaller doses per fraction). In order to attain this goal, the BED must be consistently evaluated from one set of parameters that are material constants throughout the investigated dose range. This is not the case with the LQ model, as can be inferred from Figure 4A. Namely, as seen on Figure 4A, beyond 10 Gy, from the lack of agreement between cell-surviving fractions from the LQ model and measurement, it follows that BED_{LQ} based on only one fixed value of the ratio β/α is inapplicable to the entire dose range of interest, D = 0–18 Gy. In other words, to obtain the BED, which closely conforms to the experimental data at all doses from 0 to 18 Gy, the interval (0–18) Gy should be split into two sub-ranges: (0–10) Gy and (10–18) Gy. This should be subsequently followed by two separate computations of the variance from $S_F(D)$ in the LQ model and the experimental data. The ensuing results might eventually give a reasonable agreement between the surviving fractions in the LQ model and the corresponding measurements, with the price of having two sets of the quotients β/α, one for (0–10) Gy and the other for (10–18) Gy. Such a dose-range dependence of the ratio β/α automatically yields the associated dose-range dependence of BED_{LQ}. This latter dose-range dependence precludes any meaningful inter-comparisons of different fractionation regimens (e.g., small versus large doses per fraction) and in fact undermines the value of the true concept as well as usefulness of the biologically effective dose.

The concept of the BED could be restored by having a single set of parameters that are dose-range independent, as is indeed the case in the PLQ model via $BED_{PLQ}=(1 + \beta D/\alpha)/(1 + \gamma D)$. In this latter expression, parameters α, β and γ are the same for the whole dose range (0–18) Gy. This is possible because these parameters are obtained by the PLQ model in a single reconstruction at all doses without subdividing the whole dose interval (0–18) Gy into two segments (0–10) Gy and (10–18) Gy. Hence, rather than exclusively relying on the BED_{LQ}, as is currently the case, the biologically effective dose BED_{PLQ} in the PLQ model should be used in dose-planning systems as well as in inter-comparisons among different fractionation schedules in clinical practice. This suggested replacement of $BED_{LQ} = 1 + \beta D/\alpha$ by $BED_{PLQ} = (1 + \beta D/\alpha)/(1 + \gamma D)$ entails only one additional parameter (γ). However, this is only a minor inconvenience, since this extra parameter γ is given by βD_0, where the mean lethal dose D_0 can readily be extracted from the slope $k_0 = 1/D_0$ of the straight line for the terminal part of the analyzed experimental cell survival curve $S_F(D)$ in a semi-logarithmic plot.

CONCLUSIONS

Molecular imaging will profoundly impact on all aspects of clinical decision making for patients with cancer. Among the most critical of these aspects are staging, assessment of prognosis, choice of initial therapy, target definition, determination of the need for boost doses in radiation therapy, follow-up, and eventual salvage therapy. The key step will be to develop new algorithms informed by the results of molecular imaging, which could then become the norm for personalized cancer medicine. Improved early detection, especially among persons at high risk for specific cancers, is anticipated via molecular imaging through magnetic resonance, especially with the application of optimized signal-processing methods.

Acknowledgments

This work was supported by Cancerfonden, King Gustav the 5th Jubilee Fund, Stockholm City Council (FoUU) Fund and the Karolinska Institute Research Fund, to which the authors are grateful.

Corresponding author:
Dr. K. Belkić
Dept. of Oncology-Pathology, Karolinska Institute, Building p-9, 2nd floor, Box 260, Stockholm SE-17176, Sweden
Phone: (46-8) 517-72184
email: Karen.Belkic@ki.se

BED = biologically effective dose

References

1. Jones T. The spectrum of medical imaging. *Eur J Cancer* 2002; 38: 2067-9.
2. Pinker K, Stadlbauer A, Bogner W, et al. Molecular imaging of cancer: MR spectroscopy and beyond. *Eur J Radiol* 2012; 81: 566-77.
3. Kircher MF, Hricak H, Larson SM. Molecular imaging for personalized cancer care. *Molec Oncol* 2012; 6: 182-95.
4. Seigneurin A, Exbrayat C, Labarère J, et al. Association between diagnostic work-up with subsequent attendance in a breast cancer screening program for false-positive cases. *Breast Cancer Res Treat* 2011; 127: 221-8.
5. Fitzpatrick P, Fleming P, O'Neill S, et al. False-positive mammographic screening: factors influencing re-attendance over a decade of screening. *J Med Screen* 2011; 18: 30-3.
6. Berg WA, Blume JD, Adams AM, et al. Reasons women at elevated risk of breast cancer refuse breast MR imaging screening: ACRIN 6666. *Radiology* 2010; 254: 79-87.
7. Brandt A, Lorenzo Bermejo J, et al. Breast cancer risk in women who fulfill high-risk criteria: at what age should surveillance start? *Breast Cancer Res Treat* 2010; 121: 133-41.
8. Juweid ME, Stroobants S, Hoekstra OS, et al. Use of positron emission tomography for response assessment of lymphoma: consensus of the Imaging Subcommittee of International Harmonization Project in Lymphoma. *J Clin Oncol* 2007; 25: 571-8.
9. von Schulthess GK, Steinert HC, Hany TF. Integrated PET/CT: current applications and future directions. *Radiology* 2006; 238: 405-22.
10. Madani I, Duthoy W, Derie C, et al. Positron emission tomography-guided, focal-dose escalation using intensity-modulated radiotherapy for head and neck cancer. *Int J Radiat Oncol Biol Phys* 2007; 68: 126-35.
11. van Loon J, Offermann C, Bosmans G, et al. ^{18}FDG-PET based radiation planning of mediastinal lymph nodes in limited disease small cell lung cancer changes radiotherapy fields: a planning study. *Radiother Oncol* 2008; 87: 49-54.
12. Rischin D, Peters L, O' Sullivan B, et al. Tirapazamine, cisplatin, and radiation versus cisplatin and radiation for advanced squamous cell carcinoma of the head and neck. *J Clin Oncol* 2010; 29: 2989-95.
13. Troost EG, Vogel WV, Merkx MA, et al. ^{18}F-FLT PET does not discriminate between reactive and metastatic lymph nodes in primary head and neck cancer patients. *J Nucl Med* 2007; 48: 726-35.
14. Wållberg H, Grafström J, Cheng Q, et al. HER2-positive tumors imaged within 1 hour using a site-specifically 11C-labeled Sel-Tagged affibody molecule. *J Nucl Med* 2012; 53: 1446-53.
15. Hanahan D, Weinberg RA. Hallmarks of cancer: the next generation. *Cell* 2011; 144: 646-74.
16. Kwock L, Smith J, Castillo M, et al. Clinical role of proton magnetic resonance spectroscopy in oncology: brain, breast and prostate cancer. *Lancet Oncol* 2006; 7: 859-68.
17. Morita N, Harada M, Otsuka H, et al. Clinical application of MR spectroscopy and imaging of brain tumor. *Magn Reson Med Sci* 2010; 9: 167-75.
18. Kauppinen R, Peet AC. MRI and MRS in cancer diagnostics and monitoring: preclinical and clinical approaches. *Cancer Biol Ther* 2011; 12: 665-79.
19. Begley JK, Redpath TW, Bolan PJ, et al. In vivo proton magnetic resonance spectroscopy of breast cancer: a review of the literature. *Breast Cancer Res* 2012; 14: 207-17.
20. Belkić Dž. Exact quantification of time signals in Padé-based magnetic resonance spectroscopy. *Phys Med Biol* 2006; 51: 2633-70.
21. Belkić Dž, Belkić K. Signal Processing in Magnetic Resonance Spectroscopy with Biomedical Applications. Boca Raton: CRC Press Taylor & Francis Group, 2010.
22. Katz-Brull R, Seger D, Rivenson-Segal D, Rushkin E, Degani H. Metabolic markers of breast cancer: enhanced choline metabolism and reduced choline-ether-phospholipid synthesis. *Cancer Res* 2002; 62: 1966-70.
23. Eliyahu G, Kreizman T, Degani H. Phosphocholine as a biomarker of breast cancer: molecular and biochemical studies. *Int J Cancer* 2007; 120: 1721-30.
24. Glunde K, Jie C, Bhujwalla Z. Molecular causes of the aberrant choline phospholipid metabolism in breast cancer. *Cancer Res* 2004; 64: 4270-6.
25. Belkić K, Belkić Dž. Possibilities for improved early breast cancer detection by Padé-optimized magnetic resonance spectroscopy. *IMAJ* 2011; 13: 236-43.
26. Pouliot J, Kim Y, Lessard E, et al. Inverse planning for HDR prostate brachytherapy used to boost dominant intraprostatic lesions defined by magnetic resonance spectroscopy imaging. *Int J Radiat Oncol Biol Phys* 2004; 59: 1196-207.
27. Belkić Dž, Belkić K. A meta-analysis of studies using MR spectroscopy for evaluating suspicious lesions after radiation therapy of primary brain tumors. *J Math Chem* 2012; 5: 2527-57.
28. Meisamy S, Bolan PJ, Baker EH, et al. Neoadjuvant chemotherapy of locally advanced breast cancer: predicting response with in vivo 1H MR spectroscopy – a pilot study at 4T. *Radiology* 2004; 233: 424-31.
29. Sankar T, Caramanos Z, Assina R, et al. Prospective serial proton MR spectroscopic assessment of response to tamoxifen for recurrent malignant glioma. *J Neuro-Oncol* 2008; 90: 63-76.
30. Laprie A, Catalaa I, Cassol E, et al. Proton magnetic resonance spectroscopic imaging in newly diagnosed glioblastoma: predictive value for the site of post-radiotherapy relapse in a prospective longitudinal study. *Int J Radiat Oncol Biol Phys* 2008; 70: 773-81.
31. Ladd SC. Whole-body MRI as a screening tool? *Eur J Radiol* 2009; 70: 452-62.
32. Drzezga A, Souvatzoglou M, Eiber M, et al. First clinical experience with integrated whole-body PET/MR: comparison to PET/CT in patients with oncologic diagnoses. *J Nucl Med* 2012; 53: 845-55.
33. Askoxylakis V, Dinkel J, Eichinger M, et al. Multimodal hypoxia imaging and intensity modulated radiation therapy for unresectable non-small-cell lung cancer: the HIL trial. *Radiat Oncol* 2012; 7: 157-63.
34. Tzikas A, Karaiskos P, Papanikolaou N, et al. Investigating the clinical aspects of using CT vs. CT-MRI images during organ delineation and treatment planning in prostate cancer radiotherapy. *Technol Cancer Res Treat* 2011; 10: 231-42.
35. Belkić Dž, Belkić K. Padé-Froissart exact signal-noise separation in nuclear magnetic resonance spectroscopy. *J Phys B* 2011; 44: 125003.1-16.
36. Cramp WA, Lunec J, George A, et al. The extent of bonding of newly synthesized DNA to parent template in unirradiated cells as a prediction of radiation sensitivity. *Int J Radiat Biol* 1982; 41: 193-6.
37. Belkić Dž, Belkić K. Mechanistic repair-based Padé linear-quadratic model for cell response to radiation damage. *Adv Quantum Chem* 2013; 65: 407-49.
38. Andisheh B, Edgren M, Belkić Dž, et al. A comparative analysis of radiobiological models for cell surviving fractions at high doses. *Technol Cancer Res Treat* 2013; 12: 183-92.
39. Gribbestad IS, Sitter B, Lundgren S, Krane J, Axelson D. Metabolite composition in breast tumors examined by proton nuclear magnetic resonance spectroscopy. *Anticancer Res* 1999; 19: 1737-46.
40. Swanson MG, Zektzer AS, Tabatabai ZL, et al. Quantitative analysis of prostate metabolites using 1H HR-MAS spectroscopy. *Magn Reson Med* 2006; 55: 1257-64.

"The voice of conscience is so delicate that it is easy to stifle it; but it is also so clear that it is impossible to mistake it"

Madame De Stael (1766-1817), French woman of letters of Swiss origin whose lifetime overlapped with the events of the French Revolution and the Napoleonic era. She was one of Napoleon's principal opponents

"Ultimately, the only power to which man should aspire is that which he exercises over himself"

Elie Wiesel (b. 1928), Romanian-born Jewish-American political activist, writer and Nobel laureate. He wrote 57 books, including *Night*, a work based on his experiences as a prisoner in the Auschwitz, Buna, and Buchenwald concentration camps